Flow, Turbulence and Combustion (2026) 116:20
https://doi.org/10.1007/s10494-025-00713-z

RESEARCH

Investigation of the Flow Field Morphology of Film Cooling in Supersonic Flow

Umberto Sandri[1] · Massimiliano Ferro[1] · Alessio Picchi[1] · Antonio Andreini[1] · Bruno Facchini[1] · Marc D. Polanka[2]

Received: 12 February 2025 / Accepted: 13 September 2025 / Published online: 11 December 2025

Abstract
Film cooling is widely implemented in highly thermally stressed gas turbine components. Its performance has been extensively investigated for several decades and many results are available in the literature. In conventional gas turbines, regions of supersonic flow are not prevalent and should generally be avoided. For this reason, results relative to film cooling in supersonic flow are limited. Nevertheless, a new interest related to Rotating Detonation Combustors (RDC) and supersonic turbines is growing. The implementation of those engine components in a gas turbine is likely to need film cooling for thermal protection. In this context, it becomes crucial to gain an understanding of how the film interacts with the freestream when operated in a supersonic flow. This paper investigates the effect caused by the injection of film cooling on the morphology of the supersonic flow field. Results obtained by means of schlieren imaging indicated that the coolant injection acts as a wedge inside the flow, determining the local formation of an oblique bow shock around each film cooling hole. The shape, inclination, and strength of the oblique shock showed a dependency on the fundamental dimensionless parameters considered for the characterization of the operating conditions of film cooling. Furthermore, as the amount of mass injected was increased, the inclination of the generated shocks increased and the impingement location of the reflected shock moved upstream along the injection plate. The fluid dynamics of this interaction affected the local pressure distribution on the injection plate, measured by means of Pressure Sensitive Paint (PSP). Different film cooling geometries and main flow conditions were tested at multiple operating conditions. The relative impact of the different parameters is presented, providing useful information for the design of a film cooled engine component exposed to a supersonic flow.

Keywords Film cooling · Shock waves · Pressure field · Schlieren · Pressure sensitive paint

✉ Umberto Sandri
umberto.sandri@unifi.it

[1] Department of Industrial Engineering (DIEF) University of Florence, Florence, Italy

[2] Air Force Institute of Technology, WPAFB, Dayton, OH 45433, USA

Nomenclature

$I\left(\frac{\rho_c u_c^2}{\rho_m u_m^2}\right)$ Momentum flux ratio
$BR\left(\frac{\rho_c u_c}{\rho_m u_m}\right)$ Blowing ratio
$DR\left(\frac{\rho_c}{\rho_m}\right)$ Density ratio
$VR\left(\frac{u_c}{u_m}\right)$ Velocity ratio
Ma Mach number
P Pressure
T Temperature
ρ Density
C_d Discharge coefficient
γ Heat capacity ratio
R Universal gas constant
W Molar Mass
$\dot{m}$ Coolant mass flow

Subscript and Superscript

c coolant
m Main flow
$*$ Relative to the throat
0 Total quantities

1 Introduction

Gas turbine components require both internal and external cooling to maintain their temperatures at acceptable levels. While for internal cooling several approaches can be investigated, external cooling is referred to as film cooling. This cooling technique consists of the injection of cooling air through the surface to be protected, covering it with an air film at a lower temperature. Conventional film cooling in subsonic flow has been extensively studied by the scientific community for many decades, resulting in a comprehensive understanding of its performance. For example, Bogard and Thole (Bogard and Thole 2006) provided an extensive review of film cooling performance, comparing many operating conditions such as blowing ratio (BR) as well as different geometries. Andreini et al. (2014) specifically examined the adiabatic effectiveness of perforated plates used for liner cooling. Similarly, Schroeder and Thole (2014) conducted comparable measurements on shaped film cooling holes.

In general, there are three different flow regimes of operation of film cooling: fully attached coolant jets, coolant jets detached and then reattached, and fully detached. These regimes of coolant jets' behavior were found to scale with the momentum flux ratio (I) (Bogard and Thole 2006). Namely, the first regime applies to I values up to 0.4, if $0.4 < I < 0.8$ then the coolant is in the second regime, and if I is larger than 0.8, the jet is fully detached, i.e., in the third regime. The behaviour of the jets can also be studied in terms of other dimensionless parameters, such as the blowing ratio BR, the density ratio DR, and the velocity ratio VR. If two parameters are defined, then the other two are also uniquely defined. Eberly and Thole (2013) investigated the impact of the density ratio on film cooling performance for fixed values of blowing ratios. Their results have shown that for both low and high DR (1.2

and 1.6, respectively), detachment starts to occur at BR of 1: however, in a more severe way at the lower DR. Additionally, high DR showed better lateral spreading of the jet at a given BR, thus improving the performance. This is consistent with a reduction of I for increased DR based on their definitions, i.e. increasing DR reduces I, leading to regimes of increased jet attachment. Bogard and Thole (2006) reviewed the role of the main flow Mach number on film cooling performance. Earliest studies investigating the performance of film cooling in supersonic flow date back to the 1960s when Goldstein and Eckert investigated the effect of injecting a secondary gas in a supersonic main flow at Mach 3 through a slot. Goldstein et al. (1968) furthermore investigated the performance of air injection through a porous wall into a mainstream flow at Mach 2.9. More conventional film cooling geometries for gas turbine applications have been investigated considering mainstream flow in a compressible regime. One of the initial studies in supersonic flow were performed by Wittig et al. (1996) who first introduced the blockage effect and associated shock generation due to the coolant injection in a supersonic flow. Later, Gritsch et al. (1998b) limited the investigation to the characterization of the discharge coefficient. Then, the same authors published another more extensive work investigating the adiabatic effectiveness (Gritsch et al. 1998a). The latter paper analyzed three different cooling geometries, several operating conditions, and considered both subsonic and supersonic main flow conditions (1998a). This study thus represents the first time that the effect of a supersonic main flow on discrete film cooling holes was investigated. The results show that as long as the Mach number remains well below one, the performance was independent of the Mach number. However, for the supersonic case, an improvement to the film cooling was induced by the alteration of the flow field caused by the jet injection. The phenomenon is described as the formation of a bow shock due to the obstacle in the supersonic flow induced by the jet injection. Then, according to the authors, a re-compression shock is considered to be responsible for turning the ejected jet into a flow parallel to the surface and thus improving the measured adiabatic effectiveness. The improvement is thus more relevant for high blowing ratio cases where the liftoff is impeded by the shock formations. Nevertheless, this description of the flowfield is simply inferred considering the findings of Spaid and Zukiski (1968), but was not verified by Gritsch et al. (1998a). This investigation was expanded three years later by Ligrani et al. (2001), who investigated the adiabatic effectiveness and the flowfield associated with film cooling in supersonic flow up to a Mach number of 1.12. The generated shock structure was captured with the use of shadowgraphy. While an extensive collection of effectiveness results is provided, the correlation between the adiabatic effectiveness results and the morphology of the flow field was not clearly evident. While these and other studies have investigated the effect of the film cooling in supersonic flow, few studies have sought to understand the morphology of the flow field associated with the most modern film cooling configurations for gas turbine applications. Specifically, understanding the impact that moderate levels of supersonic main flow have on the coolant jet. With a new interest in RDC, which explicitly contains supersonic flow in the detonation channel, there is a need for experimental investigations of film cooling within a supersonic cross flow. In this context, a test rig was developed at the University of Florence to allow the characterization of the performance of film cooling with an elevated freestream Mach number. Specifically, this paper investigates the morphology of the flowfield where a film cooling jet interacts with a supersonic cross flow with a schlieren setup. The shock shape and inclination downstream of the coolant jet were captured along with the jet penetration and thus its regime. Furthermore, the implementation of PSP on the injection plate allowed a map of the pressure field to be obtained. These results are linked with the schlieren ones to provide a full understanding of the flow field morphology.

2 Experimental Facility

The test rig consists of a suction type supersonic wind tunnel delivering supersonic flow to a film cooled test section. A sizing process, based on the pumping capabilities of two EU750 pumps, defined the maximum size of the test section and the Mach number that could be reached. The process led to the selection of a test section 5 cm wide and 3 cm high as indicated in Fig. 1. The test section was established downstream of a 2D convergent divergent nozzle, shaped on one side only, capable of delivering a uniform flow at Mach 1.65. Optical access was enabled on both the transversal direction through highly refined quartz windows and through the top surface, with a polished PMMA window. Film cooling holes were installed immediately after the end of the divergent section of the wind tunnel nozzle to avoid unnecessary boundary layer growth before the film cooling injection. The plenum was installed in the lower part of the tunnel. The coolant temperature and pressure were monitored by a thermocouple and a pressure probe installed in the plenum. The coolant gases were fed to the plenum through a long circuit of tubes, thus bringing the temperature to the same level as the ambient temperature. The coolant mass flow was controlled by valves and was measured with a Coriolis mass flow meter, allowing mass flows up to 12 g/s with an accuracy equivalent to 0.5% of the measured value. For the present investigation, BR values ranging between 0.5 and 4 have been considered.

Additionally, the replaceable injection plate allows investigation of different film cooling geometries. An overview of the film cooling geometries selected is shown in Fig. 2. For the present study, three film cooling hole geometries were selected to represent options for

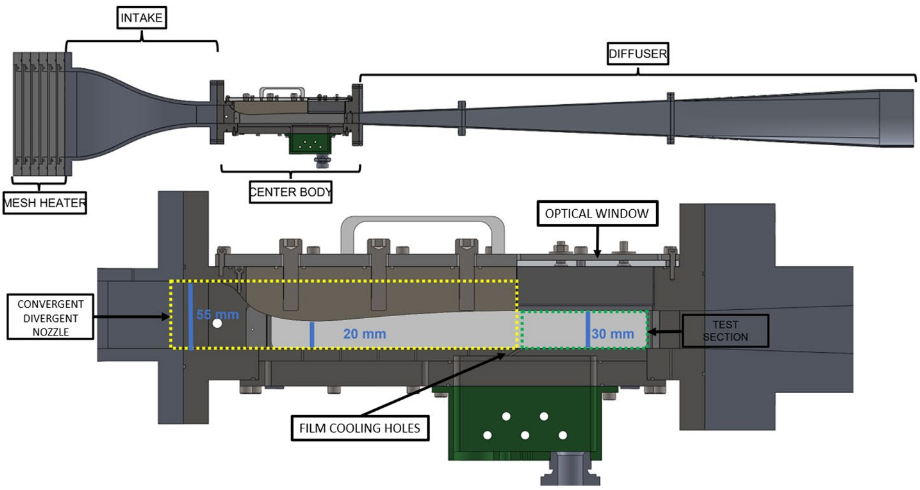

Fig. 1 Schematic of the test rig and its main components. Yellow box: convergent divergent nozzle for the conditioning of the flow. Green box: Test section where schlieren imaging and PSP measurements are performed

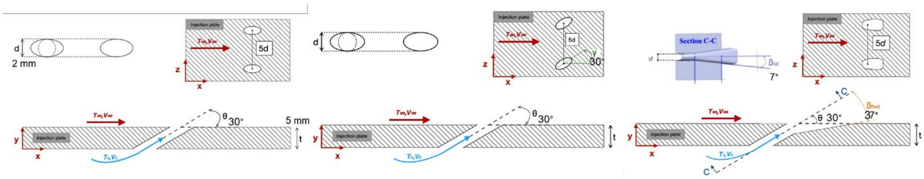

Fig. 2 Film cooling holes geometries. From the left: cylindrical holes aligned with the flow, cylindrical holes with a compound angle and 777 fan-shaped holes

cooling within an RDC. For all three geometries, a single row of film cooling holes was considered. Specifically, the present study considers cylindrical film cooling holes aligned perpendicularly to the direction of the flow with a 30-degree angle incline, similar cylindrical holes but with an additional 30-degree compound angle, and the 777 fan-shaped holes of Schroeder and Thole (Schroeder and Thole 2014). The diameter D of each hole was 2 mm, and the pitch between them was 5D for every considered geometry. The ratio of the length of the hole to the diameter was equal to six for the straight cylindrical holes. The plate thickness was kept the same in the design of the other geometries. The injection plates have been designed in such a way that all the hole geometries considered have the leading edge of the hole at the same position within the physical space of the test rig.

2.1 Schlieren Imaging

Schlieren and PSP were set up to allow the investigation of the morphology of the flow field. The schlieren technique is an optical imaging method used to visualize density changes in a transparent medium. The mode chosen for the present study was a dual schlieren system. The system was installed on an optical table, positioned transversely to the test rig, allowing for the alignment of the optical elements and providing stability. In this setup, the beam comes from a “point” source generated by a system consisting of an LED UV illuminator (IL-106UV produced by HARDsoft with a peak emission at 460 nm), a condensing lens with a focal length of 30 mm, and an orifice. The beam was then collimated by a lens placed at a distance from the point source equal to its focal length, allowing the formation of a collimated beam of light in the test section area. Downstream the test section was placed the second field lens, an achromatic lens with a diameter of 76.6 mm and a focal length of 849.9 mm. A horizontal knife edge was placed a distance equivalent to the focal length from the second field lens. Behind it, the vertical density gradients were captured by a CCD PCO 1600 b/w camera equipped with a CANON EF 75-300 mm f/4 lens.

The images acquired by the schlieren technique were post-processed via a MATLAB routine. This analysis aimed to identify the shock and expansion waves present within the test section generated by the injection of film cooling. For every operating condition, a sequence of ten images, at a frequency of 20 Hz, was captured and averaged to remove random noise. The image was then converted from pixels to cardinal coordinates via known dimensions of specific distances in the test section. The lengths were then normalized by the hole diameter, D. A supersonic freestream flow of Mach 1.65 was generated. Subsequently, different blowing ratios of coolant were produced and the angle of the resulting bow shock was observed.

For the detection of the phenomena, Lerink et al. (2020) and Smink et al. (2022) suggest a methodology based on the use of the Matlab image post-processing toolbox. First, an image obtained with no coolant emerging from the row of holes was subtracted from the images with coolant flow. This highlighted the density variations that are caused by the presence of the shock in the supersonic flow. The resulting image was then processed in three steps. First, the dynamic range of the image was increased by enhancing the contrast between different pixel intensities. Then, a filter with a 10×10 pixel window was used to create a blurred image. This image was then subtracted from the initial one, improving the sharpness. Then a normalized image was created with a mean of zero intensity and a standard deviation of one. On the processed image, binary masks were used for contour detection, allowing to capture the position of the generated oblique shock and the angle generated with the horizontal direction, together with the other features highlighted in Fig.3.

2.2 PSP Technique

Pressure sensitive paint is an experimental technique employing a paint that emits light in response to the oxygen concentration. The higher the oxygen concentration, the lower is the emission (Crafton and Fonov 2013). Since the concentration (molar fraction) of a gas in a mixture is equivalent to its partial pressure, and the concentration of oxygen in air is well known, this technique allows the calculation of the pressure field on the surface investigated, as described by Han et al. (2010).

Figure 4 shows the components required to perform the PSP measurement. Firstly, the test plate needs to be painted with PSP paint BinaryFIB provided by ISSI (Schroeder and Thole (2014)). Then, a UV illuminator is required for exciting the paint. Finally, a CCD camera, equipped with a filter with a passing band between 500 and 600 nm, was used to capture the images of the test article. Both the illuminator and camera used for the PSP technique were the same as those also used for the schlieren imaging technique. This setup allowed the collection of images with a resolution of 15.5 pixels/mm. Furthermore, the

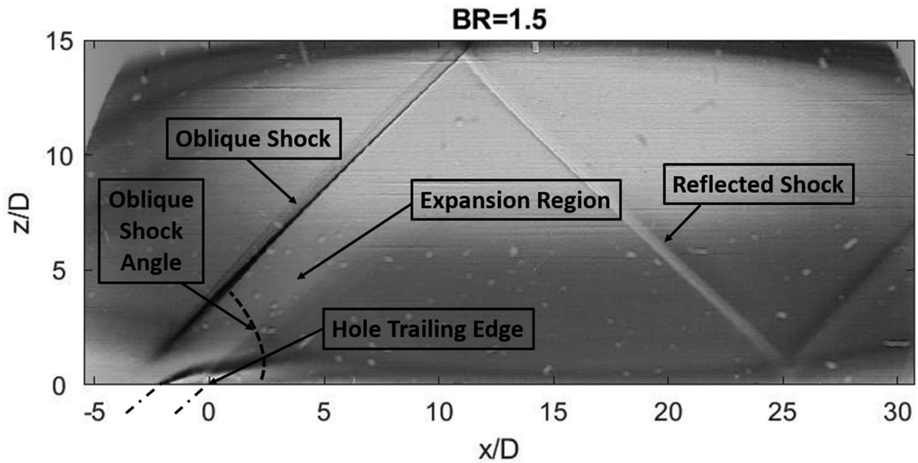

Fig. 3 Phenomena detectable by the schlieren technique

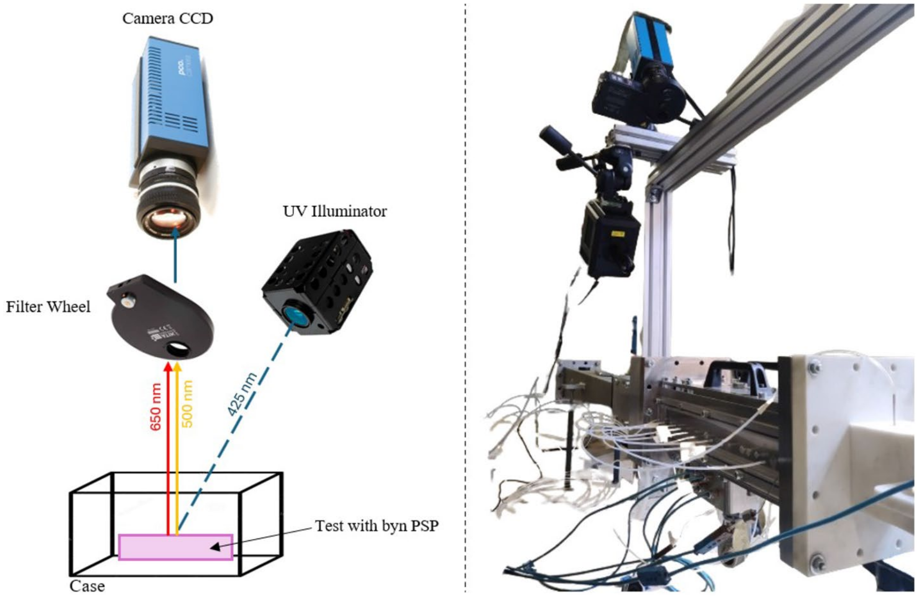

Fig. 4 Left: setup calibration scheme of PSP; Right: Setup PSP on the test rig

uncertainty of the PSP measurement is around 0.05 bar as specified by Han and Rallabandi (2010).

To evaluate the PSP signal, three images were required. First, a *dark* reference image was obtained with the illuminator turned off. Then, for each operating condition, *wind on* images were acquired with the illuminator turned on and the main flow and coolant gas activated. Then, with the illuminator still turned on, a *wind off* image was acquired with no flow in the test rig. Ten images were acquired and averaged to remove random noise, as suggested by Han et al. (Han and Rallabandi 2010). To minimize errors introduced by temperature variations, the *wind off* image was taken shortly after turning off the wind tunnel, allowing the PSP to be at the same temperature as it was during the acquisition of the *wind on* image. The images were combined to evaluate the emission intensity ratio and calculate the P/P_{ref} distribution, where P_{ref} represents the pressure of the test rig during the acquisition of the *wind off* image, i.e. the ambient pressure.

3 Results Analysis

The present study focuses on the experimental investigation of the flowfield morphology determined by the injection of film cooling in supersonic flow. Typically, to obtain adiabatic effectiveness measurements by means of PSP it is common practice to use CO_2 in the cooling flow to replicate density ratios that are representative of the real operating conditions of gas turbines. Indeed, when subsonic main flows are considered, the density ratio between coolant and main flow is determined by the ratio between the molar mass of the gas used for the coolant and the molar mass of the gas used for the main stream, which is typically air.

Thus, when air is used as coolant, the DR is equal to one, and when CO_2 is used as coolant, the DR is equal to 1.52. However, for a supersonic main flow, its low pressure results in the film cooling holes being choked. Operating with choked film cooling holes determines that the DR does not only depend on the molar weight of the gas considered for the coolant, but also on the BR selected. In this context, to understand the impact of supersonic operating conditions on the relations between a test performed using air and a test performed using CO_2, the ratio of the density ratios between the two tests is needed. It can be shown that the ratio of the density ratios between operating conditions using CO_2 and air as coolant is equal to the ratio of the densities of the two coolants, i.e. $DR_{CO_2}/DR_{air} = \rho_{CO_2}/\rho_{air}$, where both subscripts *air* and CO_2 refer to the coolant being used.

To start the derivation for the sought expression, it must be understood that in the definition of DR, as well as for BR and the other dimensionless parameters describing film cooling, the coolant quantities are defined in the cooling holes. For this reason, in case of choked flow, it is possible to express the static density as a function of the total density as follows:

$$\frac{\rho_{0,CO_2}}{\rho_{0,air}} = \frac{\rho_{CO_2} f^*(\gamma_{CO_2})}{\rho_{air} f^*(\gamma_{air})} = \frac{\rho_{CO_2}\left[\left(\frac{2}{\gamma+1}\right)^{\frac{-1}{\gamma-1}}\right]_{CO_2}}{\rho_{air}\left[\left(\frac{2}{\gamma+1}\right)^{\frac{-1}{\gamma-1}}\right]_{air}} \tag{1}$$

The expression can then be rearranged to obtain an expression for ρ_{CO_2}/ρ_{air}

$$DR_{CO_2}/DR_{air} = \rho_{CO_2}/\rho_{air} = \frac{\rho_{0,CO_2}}{\rho_{0,air}} \frac{\left[\left(\frac{2}{\gamma+1}\right)^{\frac{-1}{\gamma-1}}\right]_{air}}{\left[\left(\frac{2}{\gamma+1}\right)^{\frac{-1}{\gamma-1}}\right]_{CO_2}} \tag{2}$$

To find an expression for the ratio of the total quantities $\rho_{0,CO_2}/\rho_{0,air}$, the expression for the mass flow through a hole is utilized as follows:

$$\dot{m} = C_d A\sqrt{\rho_0 P_0 f(\gamma)} \qquad f(\gamma) = \gamma\left(\frac{2}{\gamma+1}\right)^{\frac{\gamma+1}{\gamma-1}} \tag{3}$$

Then, considering the ideal gas law, Eq. 3 can be rearranged as follows:

$$P_0 = \rho_0 \frac{R}{W} T_0 \qquad \dot{m} = C_d A\sqrt{\rho_0^2 \frac{R}{W} T_0 f(\gamma)} \tag{4}$$

Equation 4 can be defined for both air and CO_2 used as coolant gases being ejected from the plenum to the main flow. To find an expression for $DR_{CO_2}/DR_{air} = \rho_{CO_2}/\rho_{air}$ it is possible to take their ratios, obtaining the following expression:

$$\frac{\dot{m}_{air}}{\dot{m}_{CO_2}} = \frac{C_{d,air}}{C_{d,CO_2}} \frac{A_{air}}{A_{CO_2}} \frac{\rho_{0,air}}{\rho_{0,CO_2}} \sqrt{\frac{W_{CO_2}}{W_{air}} \frac{T_{0,air}}{T_{0,CO_2}} \frac{f(\gamma_{air})}{f(\gamma_{CO_2})}} \tag{5}$$

It is then possible to assume that for the two gases used as coolants (air and CO_2), when the same BR is imposed, the C_d is the same, the coolant hole area A is the same, and the total temperature T_0 is also the same. Then solving for $\rho_{0,CO_2}/\rho_{0,air}$ the following expression is obtained:

$$\frac{\rho_{0,CO_2}}{\rho_{0,air}} = \sqrt{\frac{f(\gamma_{air})}{f(\gamma_{CO_2})}\frac{W_{CO_2}}{W_{air}}} \tag{6}$$

Substituting the newly found expression for $\rho_{0,CO_2}/\rho_{0,air}$ in Eq. 2, the following expression for DR_{CO_2}/DR_{air} is obtained.

$$DR_{CO_2}/DR_{air} = \rho_{CO_2}/\rho_{air} = \frac{\left[\left(\frac{2}{\gamma+1}\right)^{\frac{-1}{\gamma-1}}\right]_{air}}{\left[\left(\frac{2}{\gamma+1}\right)^{\frac{-1}{\gamma-1}}\right]_{CO_2}} \sqrt{\frac{\left[\gamma\left(\frac{2}{\gamma+1}\right)^{\frac{\gamma+1}{\gamma-1}}\right]_{air}}{\left[\gamma\left(\frac{2}{\gamma+1}\right)^{\frac{\gamma+1}{\gamma-1}}\right]_{CO_2}}} \cdot \sqrt{\left(\frac{W_{CO_2}}{W_{air}}\right)} \tag{7}$$

Finally, with some algebraic simplification, the following final expression is derived:

$$DR_{CO_2}/DR_{air} = \rho_{CO_2}/\rho_{air} = \sqrt{\frac{\left(\frac{2\gamma}{\gamma+1}\right)_{air}}{\left(\frac{2\gamma}{\gamma+1}\right)_{CO_2}}} \cdot \sqrt{\left(\frac{W_{CO_2}}{W_{air}}\right)} \tag{8}$$

A model has been used to verify that the coolant gas is expected to be operating in choked flow conditions starting from BR 0.4. In those conditions, Eq. 8 defines the value of the ratio of the density ratios, which remains equal to 1.26 for any blowing ratio value above 0.4.

For the schlieren images, BR values of 0.5, 0.8, 1.0, 1.2 and 1.5 were acquired with both air and CO_2, allowing for a comparison of the morphology of the flow field obtained between the two gases. Then, higher blowing ratios up to BR=4 were obtained for the air coolant. For PSP measurements only air was used, as CO_2 injection does not allow for the measurement of the pressure field. Also, PSP measurements are only performed on the baseline geometry of straight cylindrical film cooling holes. PSP measurements provide insight into the impact of the shock structures visualized with schlieren on the surface pressure distribution. Additional tests were performed with only a single cooling hole. For these cases, blowing ratios up to seven were reached. These higher values of blowing ratio, beyond those typically considered for gas turbine application, allowed a thorough understanding of the underlying physics.

3.1 Schlieren Imaging

Figure 5 shows the schlieren images obtained for the three considered geometries for blowing ratios ranging between 0.5 and 1.5. The origin of the horizontal axis is placed at the exit of the film cooling holes for the cylindrical holes, and it is not changed for all of the different cooling hole geometries considered, thus causing the x/D=0 relative to the fan-shaped

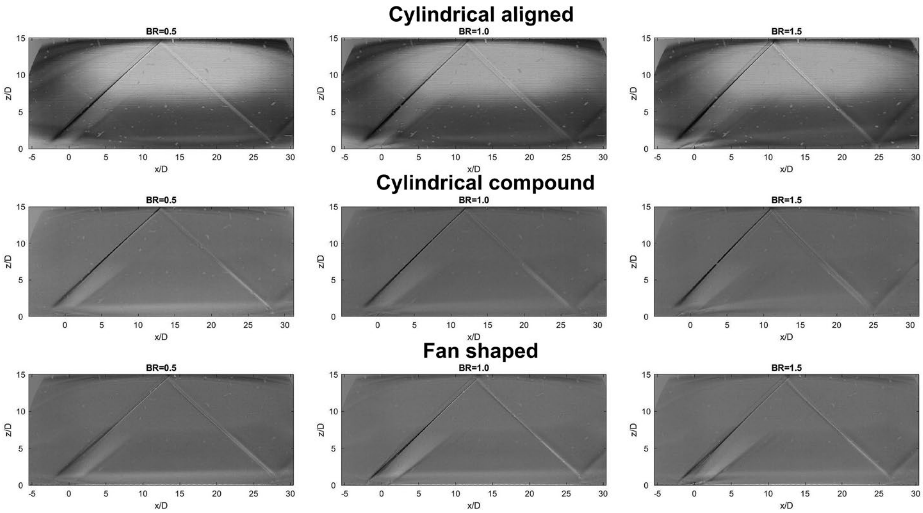

Fig. 5 Schlieren images relative to three geometries and three levels of BR typically encountered in gas turbines

hole to lie within the hole aperture itself. The results obtained are similar for the cylindrical holes aligned with the main flow and those with a compound angle. This is probably linked to both having the same exit velocity at the hole exit, and thus the same jet momentum for the jets. When the fan-shaped hole is considered, the impact location of the reflected shock is slightly downstream, indicating a lower angle of the shock wave generated by the coolant injection. The expansion at the outlet causes a velocity reduction downstream of the cooling hole minimum throat section and a lower variation of the angle of the generated oblique shock.

Similarly, Fig. 6 presents the images obtained for the same three geometries at higher BR, beyond the typical range for aeronautical applications. These results are useful to gain further insight into the physics of the phenomena observed, as they become more extreme at high BRs. At the reference BR of 3, the penetration of the jet, as highlighted by the red dashed lines in Fig. 6 has been determined visually from the Schlieren images. For the two types of cylindrical holes, the jet penetrated deeper into the main flow, reaching the height of three diameters at the axial location of five diameters downstream of the cooling holes. For the fan-shaped holes, where the outlet expansion reduces the jet penetration, the jet only reached a height of 1.5 diameters at the same location downstream.

With these images, the inclination of the oblique shock waves were determined as previously described. Figure 7 shows the variation of shock wave angle for increasing BR values for the cylindrical holes. The shock wave angle increases nearly linearly with the blowing ratio. To gain insight into the mechanism, it is useful to look at the shock polar for oblique shocks. The film injection process acts as a wedge to the incoming flow. Equation 9 relates the flow Mach number M and the oblique shock wave angle β, allowing the computation of the equivalent wedge angle θ. Fig.7 also shows the equivalent wedge angle on the second Y axis. As the blowing ratio increases, the shock angle increases from 43.6° where the wedge angle is 6°, up to 52.5° with a corresponding wedge angle of 12.1°.

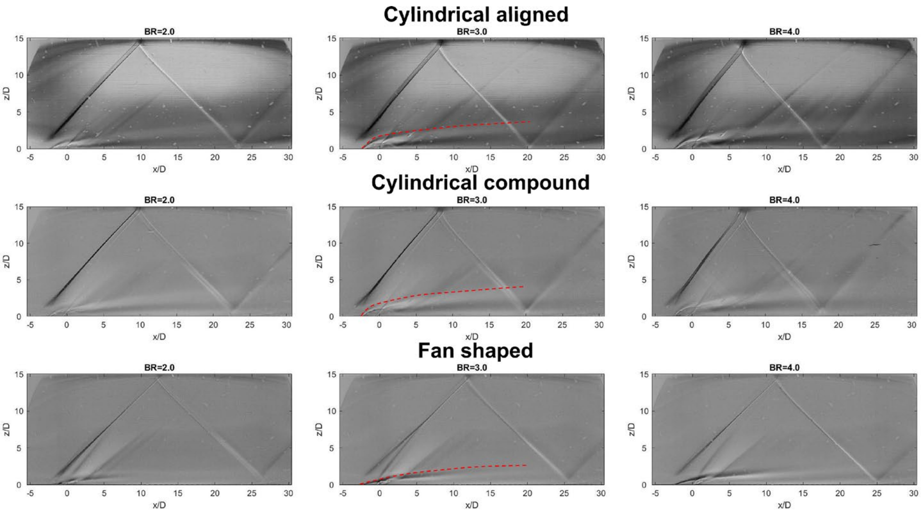

Fig. 6 Schlieren images relative to three geometries and three levels of high BR, above those typically encountered in gas turbines

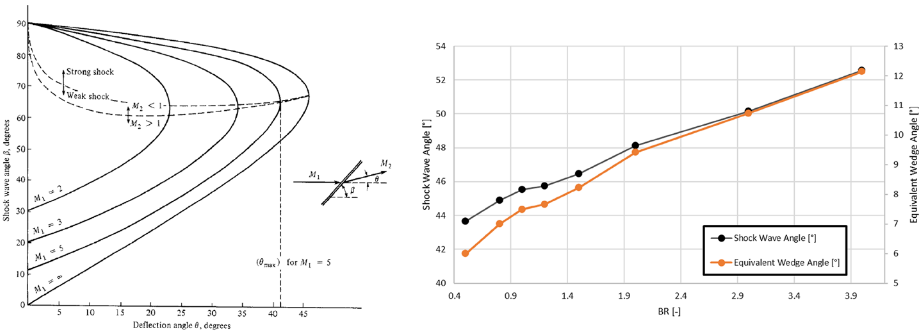

Fig. 7 On the left is the shock polar generated from Eq.9, including a representation of the terms considered in the equation (Anderson 2003). On the right is shown the variation of shock wave angle and equivalent wedge angle with increasing BR

$$tan\theta = 2cot\beta \left[\frac{M_1^2 sin^2\beta - 1}{M_1^2(\gamma + cos2\beta) - 2} \right] \tag{9}$$

Furthermore, the bow shock measured angle for the three cooling hole patterns were plotted both against BR and I in Fig. 8. For each hole, both CO_2 and air were used as coolant jets. Fig.8a shows the oblique shock wave angle as a function of BR. The trends depend on both the hole geometry and the gas considered. However, when the results are plotted against the momentum flux ratio I, the differences associated with the consideration of different gases as coolants are reduced. Indeed, Fig. 8b suggests that for a certain cooling hole geometry, the oblique shock wave angle can be uniquely determined by the momentum flux ratio I, independently of the coolant gas considered. This is consistent with I being known to be

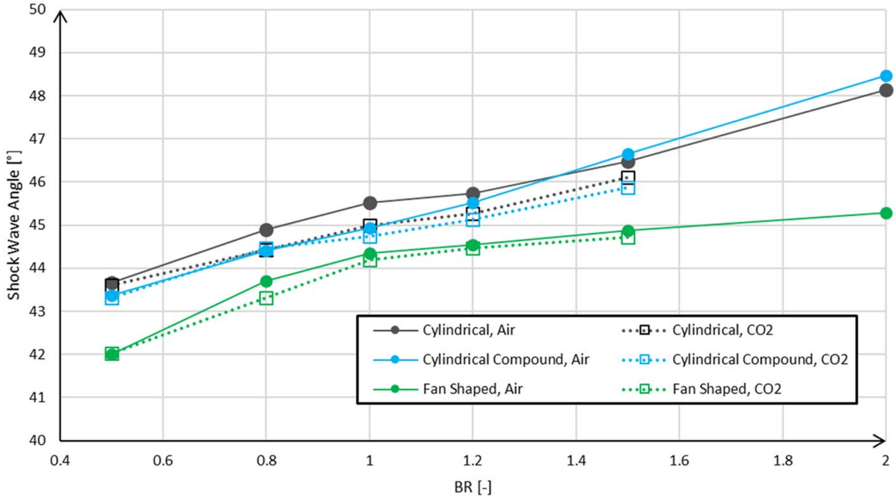

(a) Shock wave angle versus BR

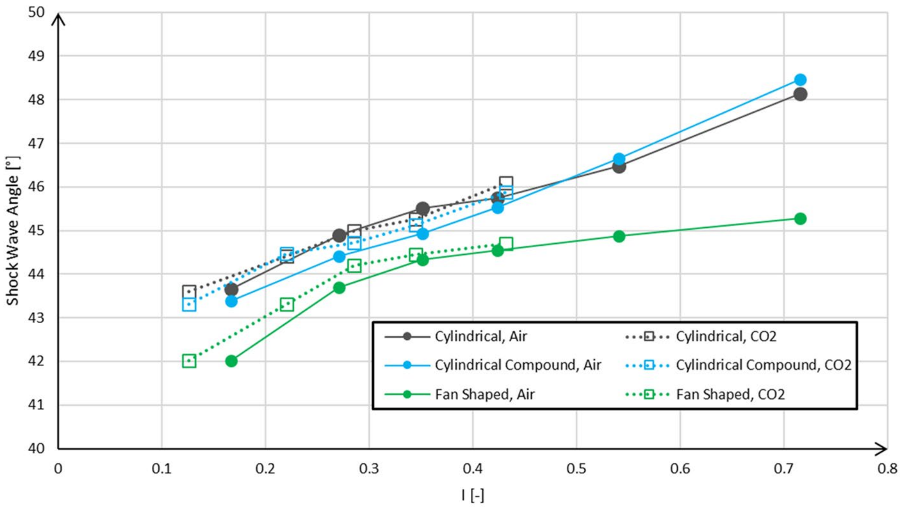

(b) Shock wave angle versus I

Fig. 8 Scaling of shock wave angle for different cooling holes geometries and different parameters. (**a**) Shock wave angle versus BR. (**b**) Shock wave angle versus I

the parameter that determines the penetration of the coolant jets as described by Thole et al. (1992)

Similar trends for the two types of cylindrical holes were expected since internally the holes present the same geometry. For the coolant operating at choked conditions inside the hole, information on the orientation of the hole does not propagate upstream inside the cooling hole itself. Furthermore, the penetration of these two configurations is expected to be the same, albeit at a different angle, thus having similar interactions with the main flow and therefore the same shock formation. Furthermore, it is clear that for the fan-shaped holes, the angle of the generated oblique shock waves was lower in comparison with the two other film cooling geometries. Such phenomena is likely to be associated with the expansion of the flow starting to occur in the divergent section inside the hole. A sketch of this scenario is presented in Fig. 9. As described in detail by Anderson (2003), when a supersonic flow encounters a deflection of the surface, the flow will turn in the new direction of the wall with an expansion wave, consisting of an infinite number of Mach waves, and the streamlines followed by the flow will be smooth curved lines.

After the choked cylindrical segment, the coolant flow has the tendency to expand with a series of expansion fans to the lower pressure of the test section, following the divergent shape of the hole. A series of expansion fans occurs at every change in angle of the diverging hole and causes a change in direction of the streamline. This smoother transition, divided in two stages, guides the flow in a direction more aligned with the injection plate as it leaves the hole, penetrating less into the main flow and determining the formation of a weaker oblique shock wave upstream and preventing separation. Such difference between the cooling holes geometry is even more evident when higher BRs are considered, as shown by the schlieren results presented in Fig. 6.

3.2 Pressure Distributions on Injection Plate

PSP measurements provide high resolution pressure distributions over the whole field of view of the camera. Figure 10 shows the pressure distribution over the complete array of five cylindrical film cooling holes with air injection. As the BR increases, the shock structure increases in intensity, generating areas of progressively higher pressure on the sides of each film hole and progressively lower pressure downstream of them. This high pressure zone is caused by the compressing action of the shock itself, which gains strength as the blowing ratio increases.

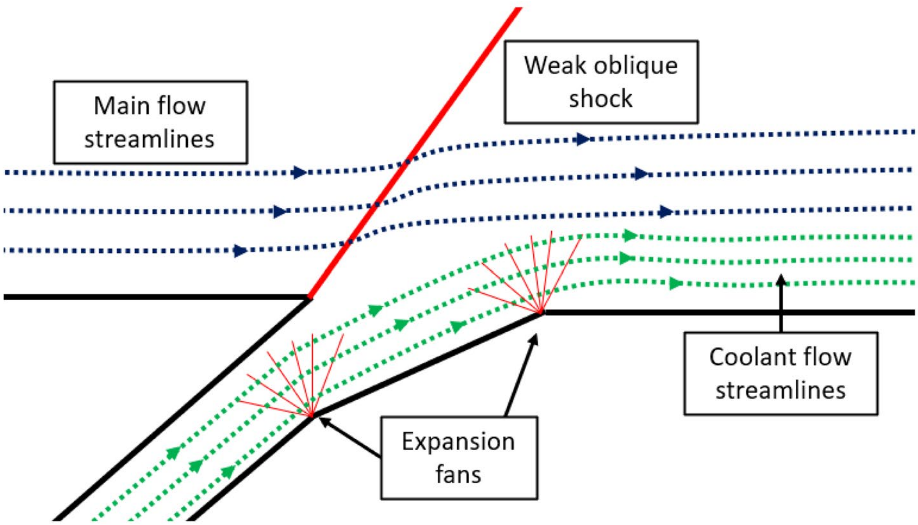

Fig. 9 Shock and expansion waves at the outlet of the fan-shaped holes

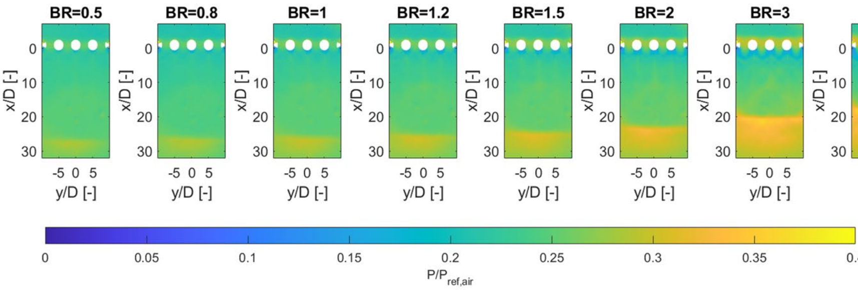

Fig. 10 Pressure distribution for increasing BR for five film cooling holes

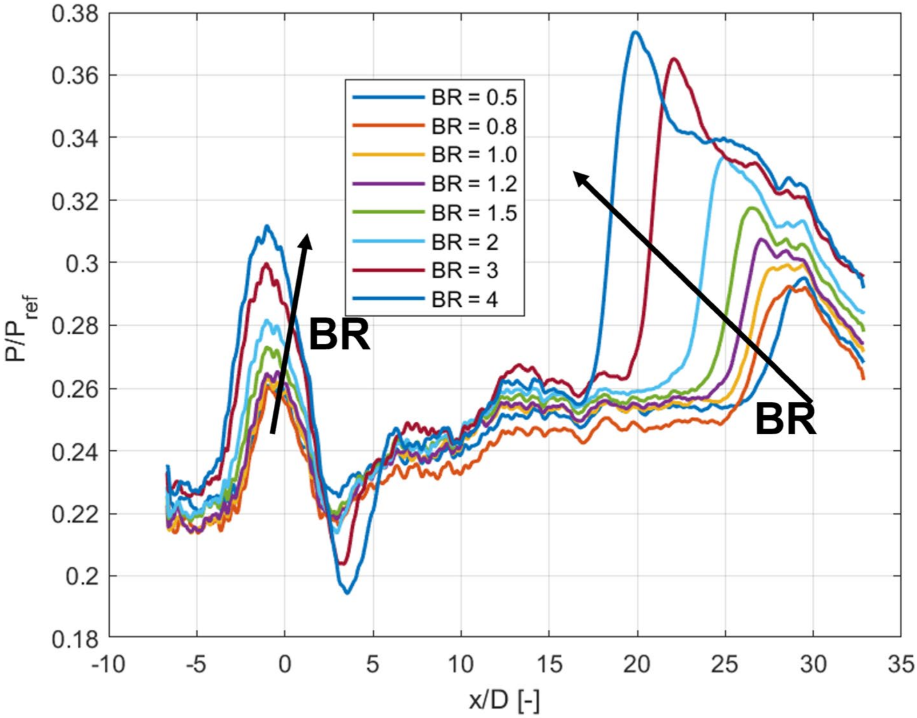

Fig. 11 Pressure profiles along the centerline between film cooling holes. Arrows indicating the variation in pressure profiles associated with an increase in BR considered

As the BR increases, the equivalent wedge angle increased and thus the inclination of the shock. More inclined shocks result in a stronger reduction of the Mach number across them and a greater pressure rise. For the higher blowing ratios, the adjacent cooling holes start to merge into a 2D planar oblique shock structure.

In addition, the zone of interaction of the reflected shock with the film injection plate moves upstream, consistent with the results identified by means of Schlieren imaging. The impingement location of the reflected shock is visible as the dark yellow region in Fig. 10. Figure 11 represents the centerline pressure over the length of the plate. In this figure, the growth in intensity of the pressure rise at the reflected shock impingement location is consistent with a gain in strength of the generated oblique shocks. The location of shock reflection is at x/D = 27 when the BR = 0.5 and moved upstream towards x/D = 17 as the BR increases to four. Comparing these profiles with the schlieren images relative to the cylindrical holes aligned with the flow presented in Fig. 5 and Fig. 6, it is clear that there is consistency between the impact location and the peak in the pressure rise. Indeed, where according to the schlieren images occurs the impact of the oblique shock, corresponds to the location where the pressure starts rapidly increasing, until reaching the peak a few diameters downstream. The physics of shock wave and boundary layer interaction is described in detail by Zuo et al. (2023). Their results also indicated an increase in the pressure rise associated with an increase in the strength of the shock. Furthermore, the increase in pressure, expected to occur slightly upstream of the impact location, occurs here in correspondence to the shock impingement. Nevertheless, such detailed investigation pertains to the specific topic of shock wave-boundary layer interaction and goes beyond the scope of the present paper.

To gain further insight into the morphology of the flowfield, tests using only the center cooling hole were performed. The other holes were closed from below with duct tape. Figure 12a) presents the results obtained for low blowing ratio values. With only a single hole, the bow shock is clearly visible as it wraps around the single central jet. To capture more clearly the phenomenology, higher blowing ratios ranging between two and seven were investigated, and the pressure maps are shown in Fig. 12b). The results are consistent with the numerical work of Pudsey and Russel (2010). In their study, the holes were vertical however, the effects were comparable.

In Fig. 12, the area of high pressure generated by the bow shock surrounds the whole film cooling hole and protrudes in the direction of the flow with a curvilinear shape. The

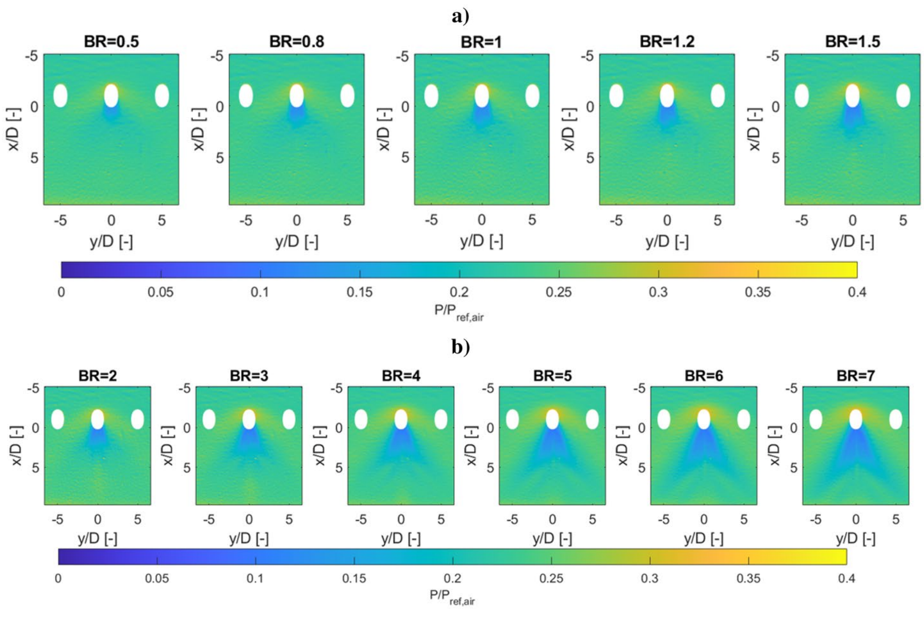

Fig. 12 Pressure distribution for increasing BR for one film cooling hole, **a**) typical BR values encountered in turbomachinery, **b**) high BR values

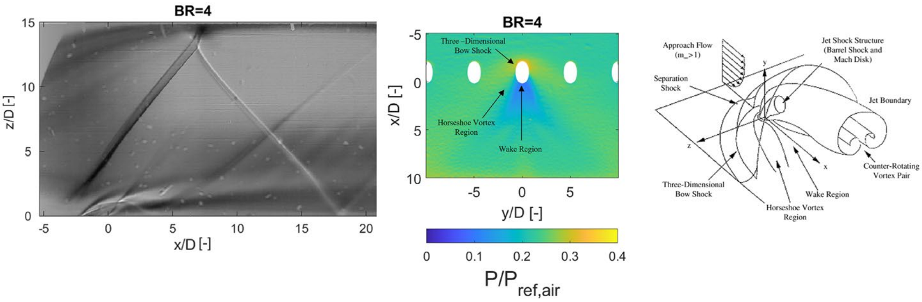

Fig. 13 Comparison between schlieren image, measured pressure distribution, and theoretical shock system morphology (Pudsey and Boyce 2010)

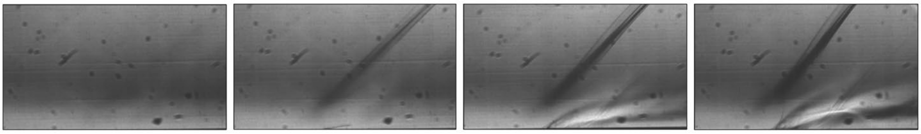

Fig. 14 Schlieren images relative to cylindrical holes for increasing BR, starting from BR = 0 to BR = 10

peak intensity was adjacent to the inlet of the film cooling hole for all the BR considered. In addition, as the BR increases, the intensity of the high pressure peak increases both in magnitude and spatial extension. Those features support, respectively, the variation of inclination associated with an increasing BR and also the bow shock shape. In addition, according to Gruber et al. (Gruber et al. 1996), the three-dimensional bow shock interacts with the boundary layer, causing it to separate and the subsequent formation of a horseshoe vortex around the jet. Furthermore, comparing the pressure distributions relative to the injection through a single hole shown in Fig. 12 and those relative to the complete array of holes shown in Fig. 10, it is possible to understand how the main features identified interact. It is apparent that while the high pressure area upstream of the holes and the horseshoe vortexes downstream are identified in both cases, the interactions of these features between the holes are different. When the whole array of holes is considered, the bow shocks upstream of each individual hole merge with each other, creating a planar oblique shock wave. On the other hand, the counter-rotating horseshoe vortexes interact with each other, canceling out their effect due to the opposite direction of rotation when neighboring ones from two adjacent holes are considered.

Finally, a comparison between the jet formation described by Gruber et al. (1996) and the pressure distribution on the injection plate is shown in Fig. 13. Consistent with their findings, a peak in pressure (yellow region) was identified upstream of the vortex, while a low pressure zone (blue region), associated with the formation of a wake or recirculation region, was formed downstream, causing a downward pitching moment.

Figure 14 shows the development of a separated bow shock forming upstream of the hole. These successive images show the weak shock that exists due to the presence of the hole developing into a stronger shock at an increased angle as the blowing ratio through the hole increases. A combination of expansion waves were subsequently generated downstream of the hole. These features are similar to the canonical vertical jet in supersonic cross flow as provided by Gruber et al. (1996)

4 Conclusions

This work investigated the morphology of the flowfield associated with the implementation of film cooling in a supersonic flow. Schlieren imaging has been used to capture the shape of the shock waves generated by the coolant injection through three different types of film cooling holes and for several levels of blowing ratios, even beyond those typically considered for gas turbine cooling applications. These results represent the first visualization of this type of interaction available in the literature. The flow injection was shown to act as an obstacle in the main flow, causing the formation of weak oblique shock waves. Quantitative data have been used to identify a strong correlation between the blowing ratio and the inclination of the shock induced by the jet, which acts as a progressively more inclined wedge in the supersonic flow. Additionally, results indicated that fan-shaped holes result in the formation of a weaker oblique shock, due to the coolant expansion in the downstream section of the holes, modifying the trajectory of the coolant. Fan-shaped holes showed the capability of maintaining the coolant closer to the surfaces, promising enhanced film cooling protection capabilities when compared with cylindrical holes. On the other hand, both types of cylindrical holes have shown the tendency to separate as the blowing ratio increases. This resulted in poor performance at high BR, representing a typical behavior identified in conventional applications with subsonic main flow conditions.

The structures previously presented in the literature for vertically oriented injection have been visualized with the use of Pressure Sensitive Paints. Since the holes are discrete, the wedge-like structure does not extend throughout the entire width of the test section. By visualizing a single film cooling hole, the dominant features have been clearly identified, showing the bow-like shock structure. When the whole array of film cooling holes was considered, PSP results show that the bow shocks interact with each other, causing the shock structures to merge, partially losing a three-dimensional configuration and globally acting as a 2D planar oblique shock. The impact of the reflection of the generated shock back onto the injection plate has also been investigated. Peaks in pressure profiles captured with PSP are well aligned with the impact location identified by schlieren images. The results have indicated a pressure rise associated with the impact of the reflected shock on the already disrupted boundary layer developing on the injection plate. Overall, the present study has provided additional understanding of the dominant features of film cooling in supersonic flow, providing support for the optimal design of film cooling arrays for supersonic main flow applications.

Author Contributions U.S. is the main author. The publication is part of his PhD work, and he carried out most of the research, managing the development of the study and performing the experiments and analysis. M.F., an MSc student supervised by U.S., supported the setup of the experimental techniques and contributed to post-processing activities. M.D.P. supervised the activity closely, contributed to defining the content and presentation of the work, reviewed the manuscript, and assisted in preparing several figures. B.F., as primary supervisor, and A.A., as co-supervisor, oversaw the project and provided scientific guidance throughout its development. A.P., responsible for the laboratory, offered essential support in troubleshooting the experimental setup and participated actively in the manuscript revision.

Funding Open access funding provided by Università degli Studi di Firenze within the CRUI-CARE Agreement. This project has received funding from the European Union's Horizon 2020 research and innovation program under the Marie Skłodowska-Curie grant agreement No 956,803.

Data Availability No datasets were generated or analysed during the current study.

Declarations

Competing Interests The authors declare no competing interests.

References

Anderson, J.D.: Modern Compressible Flow: With Historical Perspective. Aeronautical and Aerospace Engineering Series. McGraw-Hill Education, (2003). https://books.google.it/books?id=woeqa4-a5EgC

Andreini, A., Facchini, B., Picchi, A., Tarchi, L., Turrini, F.: Experimental and theoretical investigation of thermal effectiveness in multiperforated plates for combustor liner effusion cooling. J. Turbomach. **136**(9) (2014). https://doi.org/10.1115/1.4026846

Bogard, D.G., Thole, K.A.: Gas turbine film cooling. J. Propul. Power **22**(2), 249–270 (2006). https://doi.org/10.2514/1.18034

Crafton, J., Fonov, S.: Development of pressure-sensitive paint systems for low speed flows and large wind tunnels. In: 51st AIAA Aerospace Sciences Meeting Including the New Horizons Forum and Aerospace Exposition. American Institute of Aeronautics and Astronautics, (2013). https://doi.org/10.2514/6.2013-482

Eberly, M.K., Thole, K.A.: Time-resolved film-cooling flows at high and low density ratios. J. Turbomach. **136**(6) (2013). https://doi.org/10.1115/1.4025574

Goldstein, R.J., Eckert, E.R.G., Wilson, D.J.: Film cooling with normal injection into a supersonic flow. J. Eng. Ind. **90**(4), 584–588 (1968). https://doi.org/10.1115/1.3604692

Gritsch, M., Schulz, A., Wittig, S.: Adiabatic wall effectiveness measurements of film-cooling holes with expanded exits. J. Turbomach. **120**(3), 549–556 (1998a). https://doi.org/10.1115/1.2841752

Gritsch, M., Schulz, A., Wittig, S.: Method for correlating discharge coefficients of film-cooling holes. Aiaa J. **36**(6), 976–980 (1998b). https://doi.org/10.2514/2.467

Gruber, M.R., Nejad, A.S., Chen, T.H., Dutton, J.C.: Bow shock/jet interaction in compressible transverse injection flowfields. Aiaa J. **34**(10), 2191–2193 (1996)

Han, J.-C., Rallabandi, A.P.: Turbine blade film cooling using PSP techinque. Front. Heat. Mass Transf. **1**(1) (2010). https://doi.org/10.5098/hmt.v1.1.3001

ISSI Binary Pressure Sensitive Paints ; ISSI — innssi.com. https://innssi.com/binary-pressure-sensitive-paint/. [Accessed 27-12-2024]

Ligrani, P.M., Saumweber, C., Schulz, A., Wittig, S.: Shock wave–film cooling interactions in transonic flows. J. Turbomach. **123**(4), 788–797 (2001). https://doi.org/10.1115/1.1397305

Maag, S., Hoeijmakers, H.W., Venner, C.H., Segerink, F., Offerhaus, H.: Investigation of tandem injection in supersonic flow using schlieren visualization. In: AIAA Scitech 2020 Forum. American Institute of Aeronautics and Astronautics, Reston, Virginia (2020)

Pudsey, A.S., Boyce, R.R.: Numerical investigation of transverse jets through multiport injector arrays in a supersonic crossflow. J. Propul. Power **26**(6), 1225–1236 (2010). https://doi.org/10.2514/1.39603

Schroeder, R.P., Thole, K.A.: Adiabatic effectiveness measurements for a baseline shaped film cooling hole. In: Volume **5B**: heat Transfer. American Society of Mechanical Engineers, (2014). https://doi.org/10.1115/gt2014-25992

Smink, J.S., Hoeijmakers, H.W., Venner, C.H.: Investigation behavior jet shear layer in tandem dual jet injection in supersonic crossflow from schlieren images. In: AIAA SCITECH 2022 Forum. American Institute of Aeronautics and Astronautics, (2022). https://doi.org/10.2514/6.2022-2565

Spaid, F.W., Zukoski: E.E.: A study of the interaction of gaseous jets from transverse slots with supersonic external flows. Aiaa J. **6**(2), 205–212 (1968). https://doi.org/10.2514/3.4479

Thole, K., Sinha, A., Bogard, D., Crawford, M.: Mean temperature measurements of jets with a crossflow for gas turbine film cooling application. rmtp 69–85 (1992)

Wittig, S., Schulz, A., Gritsch, M., Thole, K.A.: Transonic film-cooling investigations: Effects of hole shapes and orientations. In: Volume **4**: heat Transfer; Electric Power; Industrial and Cogeneration. GT1996. American Society of Mechanical Engineers, (1996). https://doi.org/10.1115/96-gt-222

Zuo, J., Cui, N., Li, X., Xue, J., Wei, J., Bao, W., Zhang, S.: Effects of wall thermal state on shock wave/boundary layer interaction with foreign-gas supersonic film injection. Appl. Therm. Eng. **223**, 119989 (2023). https://doi.org/10.1016/j.applthermaleng.2023.119989